Estimation of Harmonic Power Components Affected by Frequency Instability

Diego Bellan

***Abstract*—**This work deals with the statistical properties of digital real-time measurements of harmonic power components taking into account frequency instability and additive noise. Continuous monitoring of harmonic power components is an important issue as far as power quality of modern power systems is concerned. When the computational burden prevents the use of sophisticated algorithms to cope with the lack of synchronism between voltage/current waveforms and sampling, harmonic power estimate is based on the peak search in the frequency domain. In this paper, an approximate analytical approach is proposed to provide the statistical characterization of harmonic power measurements based on the peaks of voltage/current spectra. The bias and the standard deviation of harmonic power are derived as functions of the parameters of the windows used against spectral leakage, and as functions of the statistical properties of the frequency of voltage/current waveforms treated as a random variable with uniform or Gaussian distribution.

***Keywords*—**discrete Fourier transform, frequency instability, power measurement, statistical techniques.

I. Introduction

MODERN electrical power systems are characterized by increasing complexity mainly due to the so-called distributed generation (DG) and to the widespread use of non-linear loads. In particular, the use of time-varying non-linear loads requires a continuous real-time monitoring of the harmonic content in the waveforms spectra for power quality purposes (e.g., see [1]-[2]). It is well-known, however, that one of the drawbacks of DG is frequency instability/inaccuracy of the generated waveforms [3]-[4]. Therefore, as the main objective of this paper, it is of paramount importance to investigate the effect of frequency instability on the power measurements performed by digital techniques based on analog-to-digital (A/D) conversion of the waveforms and the discrete Fourier transform (DFT) usually evaluated through the fast Fourier transform (FFT). The impact of additive noise is also investigated in order to attain a complete characterization of the measurement process. In the literature a few attempts have been made along this direction. In [5] only the effect of additive noise was taken into account with respect to measurement of the average power. Active and reactive powers at harmonic components were not investigated. In other papers (e.g., see [6]-[9]) sophisticated algorithms were proposed to face the problem of unknown frequency. However, this approach is not suited to a continuous real-time monitoring due to the required computational burden.

In this paper the waveforms frequency is modeled as a random variable, and the statistical properties of harmonic power derived from the peaks in the DFT spectra of voltage and currents are derived in analytical approximate form in terms of bias and variance of the measured power.

The paper is organized as follows. The problem statement is provided in Section II. The mathematical derivations leading to the statistical characterization of the measured harmonic power are provided in Section III. Numerical validation of the analytical results is given in Section IV. Final remarks are provided in Section V.

II. Problem Statement

Power measurements under non-sinusoidal conditions can be effectively performed by resorting to digital instrumentation based on A/D conversion of voltage and current waveforms, and time-to-frequency transformation through the DFT (with the efficient FFT algorithm). Thus, active and reactive power at each frequency of interest can be readily evaluated by processing the relevant spectral lines [6].

Two main sources of uncertainty can be identified in the measurement process outlined above. First, the fundamental frequency of voltage/current waveforms is typically affected by random instability. It means that by repeating the measurement process, slightly different values of the waveforms fundamental frequency must be expected. Such frequency instability is of course emphasized for harmonic components. When the DFT is applied, the lack of synchronism between the waveforms fundamental frequency and the sampling frequency (i.e., non-coherent sampling) will result in increased uncertainty in the power measurements. The second main source of uncertainty is additive noise. Indeed, voltage/current waveforms are always affected by additive noise which propagates through A/D conversion and DFT transformation, yielding noisy spectral lines. It is expected that the impact of additive noise is larger as the amplitude of the involved harmonic spectral lines decreases. Therefore, the resulting power evaluations should be properly characterized in statistical terms by treating each power estimate as a random variable (RV).

D. Bellan is with the Department of Electronics, Information and Bioengineering, Politecnico di Milano, 20133 Milan, Italy (phone: +39-02-23993708; e-mail: diego.bellan@polimi.it).

The time-domain voltage/current waveforms are modelled as a sum of N sine waves and additive zero-mean independent noise:

$$v(t) = \sqrt{2}\sum_{h=1}^{N} V_h \cos(2\pi f_h t + \varphi_h) + n_v(t) \quad (1)$$

$$i(t) = \sqrt{2}\sum_{h=1}^{N} I_h \cos(2\pi f_h t + \vartheta_h) + n_i(t) \quad (2)$$

After A/D conversion of (1)-(2) with sampling frequency f_s, and weighted time-windowing (N_s samples in length) against spectral leakage [10]-[11], the DFT transform provides the estimates of the complex Fourier coefficients:

$$\hat{V}_n = \frac{\sqrt{2}}{N_S \mathrm{NPSG}} \sum_{k=0}^{N_S-1} v[k]w[k]\exp(-j2\pi kn/N_S), \quad (3)$$

$$\hat{I}_n = \frac{\sqrt{2}}{N_S \mathrm{NPSG}} \sum_{k=0}^{N_S-1} i[k]w[k]\exp(-j2\pi kn/N_S), \quad (4)$$

where $w[k]$ is the selected time window characterized by the related Normalized Peak Signal Gain NPSG (see Tab. I where three examples of commonly used windows are reported with the parameters exploited in this paper). The frequency index n is related to the frequency index h in (1)-(2) by $n \times \Delta f = f_h$, where $\Delta f = f_s/N_s$ is the DFT frequency resolution. Under non-coherent sampling, the relation $n \times \Delta f = f_h$ is intended as an approximate relation where n is the index such that $n \times \Delta f$ is the discrete frequency closest to f_h.

The estimates of the active and reactive power are derived from (3)-(4) as

$$\hat{P}_h = |\hat{V}_h||\hat{I}_h|\cos(arg\hat{V}_h - arg\hat{I}_h), \quad h = 1, \dots, N \quad f_h \cong n \times \Delta f \quad (5)$$

$$\hat{Q}_h = |\hat{V}_h||\hat{I}_h|\sin(arg\hat{V}_h - arg\hat{I}_h), \quad h = 1, \dots, N \quad f_h \cong n \times \Delta f \quad (6)$$

It is worth noticing that each of the RVs $\{\hat{P}_h, \hat{Q}_h\}_{h=1}^{N}$ defined by the transformations (5) and (6) is given as a function of four RVs $\{|\hat{V}_h|, |\hat{I}_h|, arg\hat{V}_h, arg\hat{I}_h\}$ for which statistical uncorrelation cannot be assumed. Indeed, it is well known that both $|\hat{V}_h|$ and $arg\hat{V}_h$ are obtained by combining the real and the imaginary parts of the relevant DFT coefficient $\hat{V}_h$, and the same is true for $|\hat{I}_h|$ and $arg\hat{I}_h$ with respect to the DFT coefficient $\hat{I}_h$. It follows that the analytical derivation of the statistical properties of the RVs $\{\hat{P}_h, \hat{Q}_h\}_{h=1}^{N}$ given in the form (5) and (6) cannot be straightforward. In the next Section an alternative form for (5) and (6) will be provided, such that the statistical characterization of active and reactive power can be analytically derived through a straightforward approach.

III. Mathematical Derivations

In this Section the mathematical derivations will be performed with reference to the active power only. Similar derivations could be performed for the reactive power. Moreover, for the sake of simplicity, the frequency index h in (5) will be dropped since the proposed approach holds for each specific frequency f_h.

The two main sources of uncertainty outlined in Section II are analyzed in the following subsections.

A. Frequency Instability

If the frequency f of a sinusoidal component in the voltage/current waveform does not equal one of the DFT discrete frequencies (i.e., the integer multiples of the frequency resolution Δf), the related spectral-line magnitude does not take its ideal value. In fact, in this case (i.e., the non-coherent sampling condition) the spectral line magnitude is weighted by the Fourier transform of the time window $w[k]$ used in (3)-(4) against spectral leakage. An approximate methodology is here introduced, consisting in the approximation of the frequency-domain behavior of each specific window by a parabolic function obtained by setting the constraint provided by the window Scallop Loss (SL) (see Fig. 1), i.e., the maximum attenuation introduced by the window at the edges $\pm \Delta f/2$ of each DFT bin [10]. From Fig. 1, assuming the n-th DFT frequency bin as the origin of the frequency axis, the normalized attenuation introduced by the window on a waveform spectral line can be readily obtained [12]:

$$y \cong 1 - \frac{4(1-SL)}{\Delta f^2} f^2 \quad (7)$$

Such attenuation is applied to both the voltage and the current spectral lines at the frequency f. Therefore, by defining

$$z = y^2 \quad (8)$$

the active power in (5) can be rewritten as

$$\hat{P} = z|\bar{V}||\bar{I}|\cos(arg\hat{V} - arg\hat{I}) \quad (9)$$

where $|\bar{V}|$ and $|\bar{I}|$ denote the non-weighted frequency-centered spectral lines.

The frequency f will be treated as a RV symmetrically distributed around the center of a DFT frequency bin $n \times \Delta f$ (see Fig. 1). Analytical derivations will be performed for two different statistical distributions of the frequency, i.e., the uniform and the Gaussian distributions.

As far as uniform distribution is considered for the frequency f, i.e., a RV uniformly distributed within an interval δf centered on the relevant frequency bin and such that $\delta f \leq \Delta f$, it follows that also z is a RV whose mean value and variance can be analytically evaluated by direct calculation as follows [13]:

$$\mu_z = \int_{-\frac{\delta f}{2}}^{\frac{\delta f}{2}} z(f)\frac{1}{\delta f} df \cong 1 - \frac{2}{3}(1 - SL)\left(\frac{\delta f}{\Delta f}\right)^2 \quad (10)$$

$$\sigma_z^2 = \int_{-\frac{\delta f}{2}}^{\frac{\delta f}{2}} [z(f) - \mu_z]^2 \frac{1}{\delta f} df \cong \frac{16}{45}(1 - SL)^2 \left(\frac{\delta f}{\Delta f}\right)^4 \quad (11)$$

where higher order terms have been neglected.

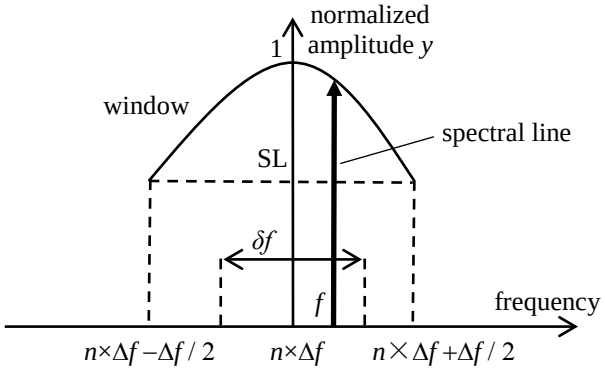

Fig. 1. Spectral line with frequency treated as a uniformly distributed RV and weighted by the frequency-domain window.

As far as a Gaussian distribution with zero mean and variance σ_f^2 is considered for the frequency f (see Fig. 2), by assuming $6\sigma_f < \Delta f$ (i.e., a distribution bounded by the frequency bin) and by using the same approach as in (10)-(11) we obtain:

$$\mu_z \cong 1 - 8(1 - SL)\left(\frac{\sigma_f}{\Delta f}\right)^2 \quad (12)$$

$$\sigma_z^2 \cong 128(1 - SL)^2 \left(\frac{\sigma_f}{\Delta f}\right)^4 \quad (13)$$

B. Additive Noise

By using a well-known trigonometric identity, the active power (9) can be rewritten as

$$\hat{P} = z|\bar{V}|\cos(arg\hat{V})\,|\bar{I}|\cos(arg\hat{I}) + z|\bar{V}|\sin(arg\hat{V})\,|\bar{I}|\sin(arg\hat{I}) = z\mathrm{Re}\{\bar{V}\}\mathrm{Re}\{\bar{I}\} + z\mathrm{Im}\{\bar{V}\}\mathrm{Im}\{\bar{I}\} \quad (14)$$

In the literature it has been shown that the real and the imaginary parts of a DFT coefficient of a noisy waveform can be treated as Gaussian uncorrelated RVs, with mean values equal to the noise-free mean values, and variances given by [14]-[17]

$$\sigma^2 = \frac{1}{N_s}\sigma_n^2 \mathrm{ENBW} \quad (15)$$

where σ_n^2 is the variance of the additive input noise, and ENBW is the Equivalent Noise Bandwidth of the selected time window.

Therefore, for the real and the imaginary parts of the voltage DFT coefficients we have:

$$\sigma_V^2 = \frac{1}{N_s}\sigma_{n_v}^2 \mathrm{ENBW} \quad (16)$$

whereas for the real and imaginary parts of the current DFT coefficients we have:

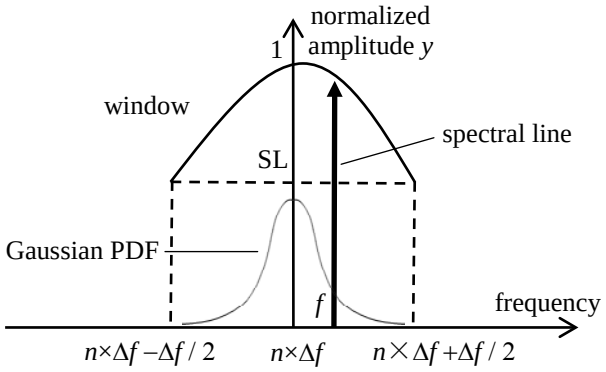

Fig. 2. Spectral line with frequency treated as a RV with Gaussian distribution and weighted by the frequency-domain window.

TABLE I.
SOME FIGURES OF MERIT OF THREE COMMON WINDOWS.

Window	NPSG	ENBW	SL [dB]	SL
Rect.	1	1	3.92	0.637
Tukey (α=0.5)	0.75	1.22	2.24	0.773
Hann	0.50	1.50	1.42	0.849

$$\sigma_I^2 = \frac{1}{N_s}\sigma_{n_i}^2 \mathrm{ENBW} \quad (17)$$

C. Mean Value and Variance Estimates

The active power in (14) is a RV given as a function of five independent RVs whose mean values and variances have been derived in the previous subsections. Therefore, approximate expressions for the mean value and the variance of $\hat{P}$ can be readily obtained by resorting to a Taylor expansion approach [13], [18]. In fact, the first-order partial derivatives (needed for the variance estimation) can be readily evaluated from (14), whereas the second-order derivatives (needed for the mean value estimation) are all zero. Thus, the mean value of $\hat{P}$ is given by:

$$\mu_{\hat{P}} \cong \mu_z P = \left[1 - \frac{2}{3}(1 - SL)\left(\frac{\delta f}{\Delta f}\right)^2\right] P \quad (18)$$

and

$$\mu_{\hat{P}} \cong \mu_z P = \left[1 - 8(1 - SL)\left(\frac{\sigma_f}{\Delta f}\right)^2\right] P \quad (19)$$

for the uniform and the Gaussian distribution, respectively. Thus, the normalized bias in the active power measurement is given by

$$b_{\hat{P}} = \frac{\mu_{\hat{P}} - P}{P} = -\frac{2}{3}(1 - SL)\left(\frac{\delta f}{\Delta f}\right)^2 \quad (20)$$

and

$$b_{\hat{P}} = \frac{\mu_{\hat{P}} - P}{P} = -8(1 - SL)\left(\frac{\sigma_f}{\Delta f}\right)^2 \quad (21)$$

The Taylor estimate for the variance in the uniform distribution case is given by:

$$\sigma_{\hat{P}}^2 \cong \sigma_z^2 P^2 + \mu_z^2(\sigma_V^2 I^2 + \sigma_I^2 V^2) =$$

$$= \frac{16}{45}(1 - SL)^2\left(\frac{\delta f}{\Delta f}\right)^4 P^2 + \quad (22)$$

$$+\left[1 - \frac{2}{3}(1 - SL)\left(\frac{\delta f}{\Delta f}\right)^2\right]^2 \frac{\text{ENBW}}{N_s}\left(\sigma_{n_v}^2 I^2 + \sigma_{n_i}^2 V^2\right)$$

whereas in the Gaussian distribution case the variance is given by:

$$\sigma_{\hat{P}}^2 \cong 128(1 - SL)^2\left(\frac{\sigma_f}{\Delta f}\right)^4 P^2 +$$

$$+\left[1 - 8(1 - SL)\left(\frac{\sigma_f}{\Delta f}\right)^2\right]^2 \frac{\text{ENBW}}{N_s}\left(\sigma_{n_v}^2 I^2 + \sigma_{n_i}^2 V^2\right) \quad (23)$$

such that the normalized standard deviations can be written as:

$$\frac{\sigma_{\hat{P}}}{P} = \sqrt{\begin{array}{c}\frac{16}{45}(1 - SL)^2\left(\frac{\delta f}{\Delta f}\right)^4 + \\ +\left[1 - \frac{2}{3}(1 - SL)\left(\frac{\delta f}{\Delta f}\right)^2\right]^2 \frac{\text{ENBW}}{N_s} \frac{\frac{\sigma_{n_v}^2}{V^2} + \frac{\sigma_{n_i}^2}{I^2}}{\cos^2(\varphi - \vartheta)}\end{array}} \quad (24)$$

and

$$\frac{\sigma_{\hat{P}}}{P} = \sqrt{\begin{array}{c}128(1 - SL)^2\left(\frac{\sigma_f}{\Delta f}\right)^4 + \\ +\left[1 - 8(1 - SL)\left(\frac{\sigma_f}{\Delta f}\right)^2\right]^2 \frac{\text{ENBW}}{N_s} \frac{\frac{\sigma_{n_v}^2}{V^2} + \frac{\sigma_{n_i}^2}{I^2}}{\cos^2(\varphi - \vartheta)}\end{array}} \quad (25)$$

respectively.

It is interesting to notice in (24) and (25) two kinds of additive contributions. The first term is strictly related to the frequency uncertainty (i.e., $\delta f/\Delta f$ and $\sigma_f/\Delta f$ in the two cases) and the SL of the window. The second term includes also the contribution of the noise-to-signal ratios $\sigma_{n_v}^2/V^2$ and $\sigma_{n_i}^2/I^2$, showing that higher-order low-amplitude harmonics result in larger uncertainty. The total noise-to-signal ratio is divided by the squared power factor $\cos^2(\varphi - \vartheta)$ which in turn can emphasize such contribution for small power factors. Moreover, as expected, the total noise-to-signal ratio is weighted by the ENBW parameter of the window, while the action of the number of samples N_s is distributing the noise power over the DFT frequency bins such that the noise impact decreases as N_s increases. Finally, it can be easily shown that the above results hold also for the reactive power.

IV. Numerical Simulations

The analytical results derived in Section III have been validated by resorting to numerical simulation of the whole measurement process. According to (1)-(2), voltage and current waveforms consisting of three harmonic components have been selected such that $f_1 = 50$ Hz, $f_3 = 3f_1, f_5 = 5f_1$. The voltage and current rms values have been selected as $V_1 = 1, V_3 = 0.1, V_5 = 0.04, I_1 = 0.5, I_3 = 0.1, I_5 = 0.02$. Phase angles 1 and 3 have been selected at random, while phase angles 5 have been given specific values since the analytical results (24)-(25) have been tested for the fifth harmonic component. Time-domain additive zero-mean Gaussian noise has been considered with $\sigma_{n_v} = \sigma_{n_i} = 0.04$. Sampling has been performed such that 10 periods of the fundamental component are acquired, i.e., a 200 ms measurement window were taken. The selection of the number of samples N_s defines the corresponding sampling frequency. By assuming $N_s = 2^{12}$ the corresponding sampling frequency is $f_s = 20.48$ kHz, and the related frequency resolution is $\Delta f = 5$ Hz. In the first set of simulations, a repeated run analysis (10^4 runs to estimate each average value) has been performed by assuming f_1 taking random values with uniform distribution within a frequency range δf centered on the nominal frequency 50 Hz. It is worth noticing that a frequency deviation δf in the fundamental component results in a frequency deviation $3\delta f$ in the third harmonic, and $5\delta f$ in the fifth harmonic. In the following, analytical results (20) and (24) have been validated for the fifth harmonic. In fact, by assuming a maximum $\frac{\delta f}{\Delta f} = 0.2$ for the fundamental component, such normalized frequency range equals 1 for the fifth harmonic. Moreover, the effect of the noise part in (24) is emphasized when low-magnitude sine-waves are considered.

In Fig. 3 the normalized bias defined in (20) is represented as a function of the normalized frequency range $\delta f/\Delta f$ for three different windows (solid lines). In the same figure, markers represent numerical estimates of the normalized bias obtained by the repeated run analysis described above, i.e., for each value of $\delta f/\Delta f$, the active power P_5 has been numerically evaluated 10^4 times by selecting the frequency at random within the range δf, and the mean value of P_5 was evaluated, allowing the calculation of the relative bias (20). Notice that even for the commonly used Hann window, a negative bias (i.e., underestimate) of 10% can be reached in the worst case where frequency instability involves the whole frequency bin Δf.

In Fig. 4 the normalized standard deviation (24) related to P_5 is validated against the numerical simulations described above. The power factor $\cos(\varphi_5 - \vartheta_5)$ has been selected equal to 1. The contribution of noise in (24) is mainly relevant to the first part of the curves, i.e., for small values of $\delta f/\Delta f$. This is proven in Fig. 5 where the power factor was decreased to 0.707 and the number of samples decreased to 1024. According to (24) this emphasizes the contribution of noise. In fact, for small values of $\delta f/\Delta f$ the standard deviation increases, whereas for larger $\delta f/\Delta f$ the behavior is the same as in Fig. 3.

A second set of simulations was performed for the Gaussian distribution of frequency. Figs. 6, 7, and 8 should be compared with Figs. 3, 4, and 5, respectively. The different shape of the Gaussian PDF with respect to the uniform PDF results in lower values for the bias and for the standard deviation of the active power.

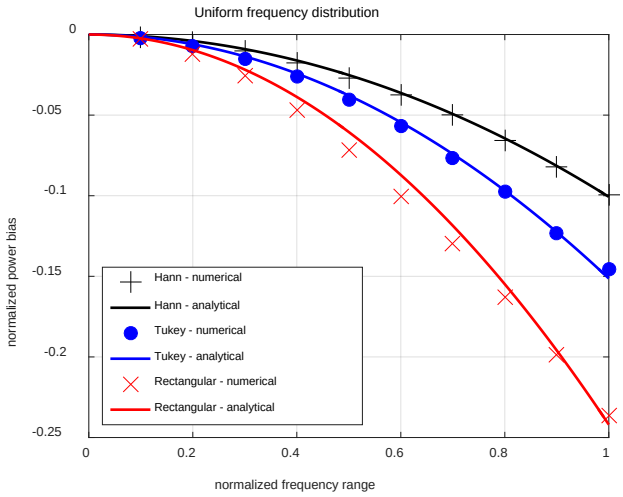

Fig. 3. Comparison between analytical and numerical bias in active power measurement due to frequency instability with uniform distribution, for three different windows.

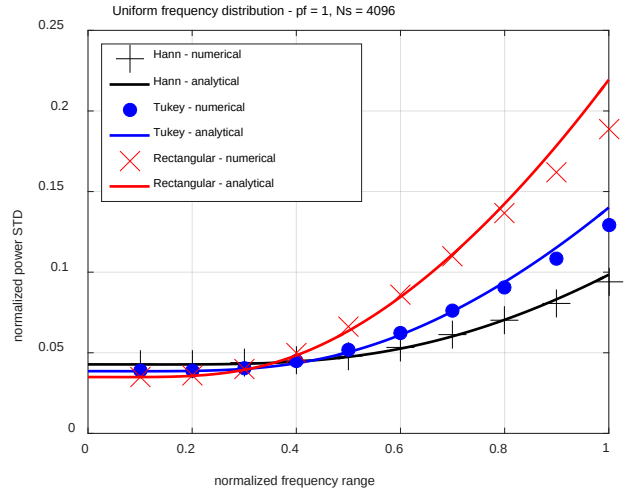

Fig. 4. Comparison between analytical (solid lines) and numerical (markers) estimates of the normalized standard deviation of P_5 (see (24)) as a function of the normalized frequency range $\delta f/\Delta f$ of the uniformly distributed frequency, for three different windows.

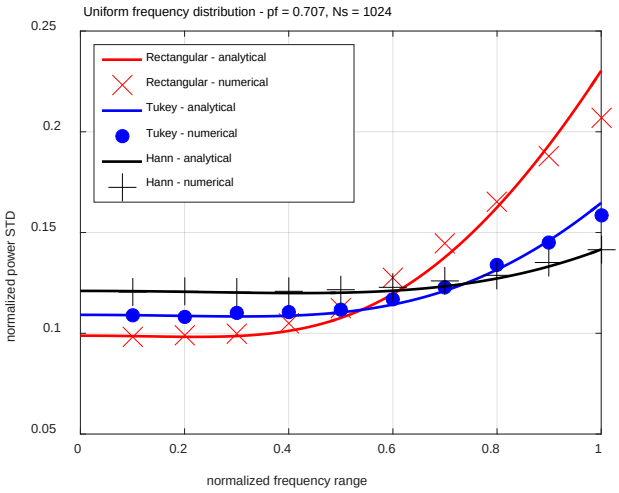

Fig. 5. Same as Fig. 4 but with decreased power factor and number of samples.

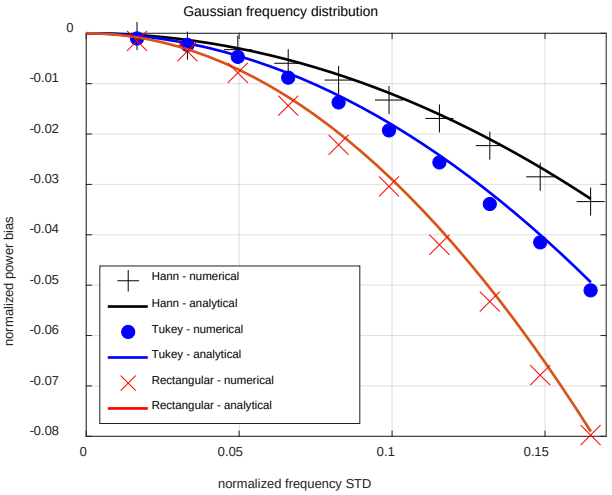

Fig. 6. Comparison between analytical and numerical bias in active power measurement due to frequency instability with Gaussian distribution, for three different windows.

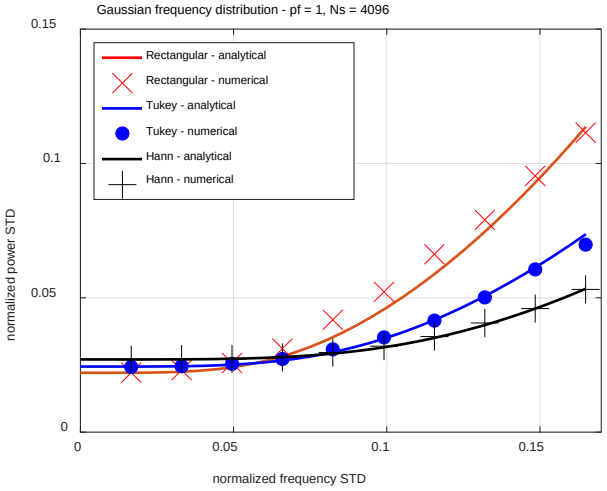

Fig. 7. Comparison between analytical and numerical estimates of the normalized standard deviation of P_5 (see (25)) as a function of the

normalized frequency standard deviation $\sigma_f/\Delta f$ of the normally distributed frequency, for three different windows.

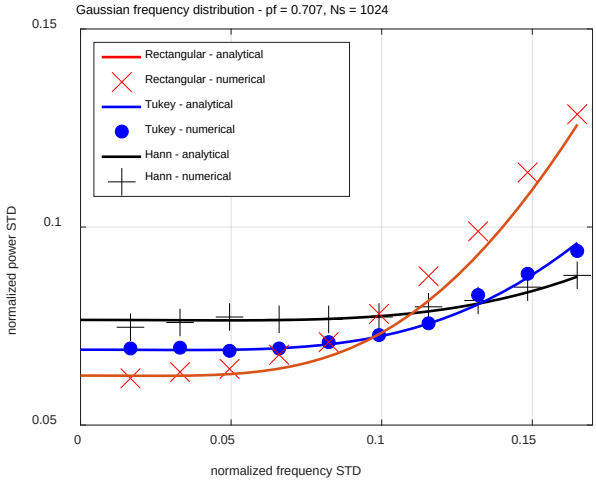

Fig. 8. Same as Fig. 7 but with decreased power factor and number of samples.

V. Conclusion

The main idea underlying the paper was the approximation of the frequency behavior of the window used against spectral leakage by a simple parabolic function, depending only on the window parameter SL. Such an approximation allowed analytical derivation of mean value and variance of harmonic power components under the assumption of uniform and Gaussian distribution of frequency. Good agreement has been obtained between analytical results and numerical simulations. The main advantage of the proposed approach is its simplicity and its capability to include most of the windows commonly used in many engineering applications. Thus, the proposed approach enables simple and straightforward statistical characterization of measured power affected by frequency instability and additive noise.

Future work will be devoted to extend the analytical results to different and possibly non-symmetrical statistical distributions for the frequency instability.

References

[1] T. Lin and A. Domijan, "On power quality indices and real time measurement," *IEEE Trans. on Power Delivery*, vol. 20, no. 4, pp. 2552-2562, 2005.

[2] D. Bellan, G, Spadacini, E. Fedeli, and S. A. Pignari, "Space-frequency analysis and experimental measurement of magnetic field emissions radiated by high-speed railway systems," *IEEE Trans. Electromagn. Compat.*, vol. 55, no. 6, pp. 1031-1042, 2013.

[3] M. H. Wang and Y. Z. Sun, "A practical, precise method for frequency tracking and phasor estimation," *IEEE Trans. on Power Delivery*, vol. 19, no. 4, pp. 1547-1552, Oct. 2004.

[4] M. R. Vedady Moghadam, R. T. B. Ma, and R. Zhang, "Distributed frequency control in smart grids via randomized demand response," *IEEE Trans. on Smart Grid*, vol. 5, no. 6, pp. 2798-2809, 2014.

[5] P. Carbone and D. Petri, "Average power estimation under nonsinusoidal conditions," *IEEE Trans. on Instrum. Meas.*, vol. 49, no. 2, pp. 333-336, April 2000.

[6] D. Agrez, "Active power estimation in the non-coherent sampling: a comparative study," in Proc. of *IMTC 2005 - Instrum. Meas. Technology Conference*, Ottawa, Canada, pp. 720-725, 17-19 May, 2005.

[7] M. Wang and Y. Sun, "A practical method to improve phasor and power measurement accuracy of DFT algorithm," *IEEE Trans. on Power Delivery*, vol. 21, no. 3, pp. 1054-1062, July 2006.

[8] T. T. Nguyen and X. J. Li, "A fast and accurate method for estimating power systems phasors using DFT with interpolation," in *Proc. 2006 IEEE Power Engineering Society General Meeting*, Montreal, Canada.

[9] D. Belega, D. Dallet, and D. Petri, "Accuracy of sine wave frequency estimation by multipoint interpolated DFT approach," *IEEE Trans. on Instrum. Meas.*, vol. 59, no. 11, pp. 2808-2815, 2010.

[10] F. J. Harris, "On the use of windows for harmonic analysis with the discrete Fourier transform," *Proc. of the IEEE*, vol. 66, pp. 51-83, 1978.

[11] O. M. Solomon, "The use of DFT windows in signal-to-noise ratio and harmonic distortion computations," *IEEE Trans. Instrum. Meas.*, vol. 43, no. 2, pp. 194-199, 1994.

[12] D. Bellan, "Frequency instability and additive noise effects on digital power measurements under non-sinusoidal conditions," in *Proc. 2014 6th IEEE Power India International Conference (PIICON)*, Delhi, India, Dec. 5-7, 2014, pp. 1-5.

[13] A. Papoulis, *Probability, random variables, and stochastic processes*, McGraw-Hill, Inc., 1991.

[14] D. Bellan, "Statistical characterization of harmonic emissions in power supply systems," *International Review of Electrical Engineering*, vol. 9, no. 4, pp. 803-810, 2014.

[15] D. Bellan, "Noise propagation in multiple-input ADC-based measurement systems," *Measurement Science Review*, vol. 14, no. 6, pp. 302-307, 2014.

[16] D. Bellan, "Characteristic function of fundamental and harmonic active power in digital measurements under nonsinusoidal conditions," *International Review of Electrical Engineering*, vol. 10, no. 4, pp. 520-527, 2015.

[17] D. Bellan, "On the validity of the noise model of quantization for the frequency-domain amplitude estimation of low-level sine waves," *Metrology and Measurement Systems*, vol. 22, no. 1, pp. 89-100, 2015.

[18] D. Bellan and S. A. Pignari, "Statistical superposition of crosstalk effects in cable bundles," *China Communications*, pp. 119-128, Nov. 2013.